2015 WJTA-IMCA Conference and Expo
November 2-4 ● New Orleans, Louisiana

Paper

PARTICLE DISINTEGRATION IN THE ABRASIVE WATER INJECTION JET

D. Zaremba, P. Heese, M. Bauer, H. J. Maier, T. Hassel
Institut für Werkstoffkunde (Materials Science), Leibniz Universität Hannover, Germany

ABSTRACT

In the Abrasive Water Injection Jet (AWIJ) process, abrasive injection is pneumatically enabled through the generation of technical vacuum by a water jet. Fed particles are collected by the jet in a mixing chamber and are subsequently accelerated. Before impact on the work piece surface, the turbulent multiphase flow containing air, water and abrasive particles is focused at a certain distance, enabling cutting applications. During acceleration and focusing, the current flow conditions provoke numerous collisions of the abrasive particles with the focusing tube. Thus, highly wear resistant materials like tungsten carbide are necessary for this component. The abrasive particles themselves are also subject to wear during collision with each other or the harder focusing tube. As a result, the actual size of the ready-to-cut particles is smaller than the original particle size.

Manufacturers of currently available machines and cutting systems tend to increase the hydraulic power through higher-pressure levels (> 500 MPa), and to minimize jet diameters for micromachining. However, the size of the particles, which carry out the actual micro chipping process, is unknown.

In this study particle disintegration in the abrasive water injection jet process was investigated. The objective was to better understand the material removal procedure during AWIJ machining. Micro- and macro cutting systems corresponding to the actual state of the art were utilized in a pressure range between 250 MPa and 550 MPa. The particle disintegration was investigated for several abrasive load ratios.

1. INTRODUCTION

In the Abrasive Water Injection Jet (AWIJ) process, the initially formed jet includes air at its surface and at the surface of its droplets, which results in a technical vacuum formed in the mixing chamber. This allows for a pneumatic transport of abrasive particles into the jet. The high-speed waterjet collects the fed particles along with a substantial amount of air in a mixing chamber and subsequently accelerates them (Figure 1). During acceleration and focusing, the flow conditions provoke collisions of the abrasive particles among themselves or with the focusing tube.

Manufacturers of currently available machines and cutting systems tend to increase the hydraulic power through higher-pressure levels ($p > 500$ MPa), and to minimize jet diameters for micromachining. These parameters have a major influence on the transport process in the focusing tube. However, due to particle wear, the size of the particles, which carry out the actual micro chipping process, is unknown. Thus, the objective of the present study was to investigate particle disintegration and contribute to understanding of the material removal procedure.

2. STATE-OF-THE-ART

The utilization of the water jet's kinetic energy as an acceleration medium for abrasive particles has a major effect on the jet's material removal behavior. The accelerated, sharp-edged abrasive particles cause the micro-chipping process. Prior to impact on the work piece surface, the turbulent multiphase flow containing air, water and abrasive particles is focused at a distance l_f ($30\ \text{mm} \leq l_f \leq 100\ \text{mm}$, dependent on orifice diameter d_o and focusing tube diameter d_f). During acceleration and focusing, the current flow conditions provoke numerous collisions. The particle acceleration direction finally results from the sum of the particles' eccentric and centric impacts among themselves, as well as with the focusing tube's cladding (1,2). Thus, highly wear resistant materials like tungsten carbide are necessary for this component. In addition to the tool wear, the abrasive particles are also subject to wear during collision between each other or with the harder focusing tube.

The accelerated particles either cause micro-chipping, micro-crenation or micro-cracking processes at the work piece. Velocity, shape and mass of the abrasive particles are important parameters that affect material removal. Criteria typically used to evaluate the material removal potential of abrasives are cutting ability, cutting quality and degree of fragmentation and particle size is a key parameter in this respect. A decrease of the particle size directly involves a decrease of cutting power because of the lower maximum momentum transfer. However, microscopic comparison of particles prior to and after the jetting process indicated a significant particle disintegration. Secondary disintegrations occur on work piece impact, as well as collisions with slowed-down particles after work-piece impact. On particle disintegration, the kinetic energy is split between the fragments. The direction of movement alters and disturbs the abrasive waterjet (2).

Since the beginning of its industrial applications, several authors have studied the Abrasive Water Injection Jet (AWIJ) process. Given the complexity of the process, most of the models developed are empirical in nature and assume given values for the particle mass or particle energy (1,3–8). In

a related study, particle disintegration has been investigated with the aim of estimating the recycling potential (2). The grade of disintegration was analyzed for three different stages (jet formation, cutting process and residual energy conversion). It was shown that the predominant disintegration takes place within the jet formation process, whereas the actual cutting process has only a minor influence in this respect. The grade of fragmentation decreases when smaller particles are used in the same cutting head (d_o = 0.25 mm, d_f = 0.9 mm, l_f = 40 mm). The grade of fragmentation ranged from 20% (d_p = 40 µm) to 60% (d_p = 600 µm) (2). However, these data were acquired with nozzle combinations that are unusual in today's industrial applications and did not consider modern ultra-high pressure and micro-cutting applications. Thus, the present study was conducted to determine the resulting particle size under such conditions and help to better understand the material removal process.

3. MATERIALS AND METHODS

3.1 Materials

Abrasives used were GMA Garnet #120 (GMA Garnet Pty Ltd, Perth, Australia) for macro applications and Barton HPX #220 (Barton Mines Co LLC, Glen Falls, NY, USA) for micro applications, technical specifications are summarized in Table 1. Initially, both abrasives were subject to a sieve analysis. According to specifications from GMA and Barton (9,10), the analysis was carried out according to DIN ISO 565 (11), series R40/3. The results were used as reference values for the following investigations, but also for verification of the particle size distribution specified by the manufacturers. For the sieve analysis, an analytical sieve shaker (manufacturer Retsch, type VS 100) was used. According to DIN ISO 565 series R40/3, the installed sieves were: 250 µm, 212 µm, 180 µm, 150 µm, 106 µm, 90 µm, 75 µm, 63 µm, 53 µm, 45 µm and 38 µm. For the gravimetric analysis, a precision balance (manufacturer Shinko, type DJ-1506, accuracy of measurements 0.001 g) was used.

All jetting experiments were carried out on a lab machine with an Engelhardt C-55 control unit. The high pressure pump was a ThyssenKrupp Uhde HPS 6045 (max. operating pressure p_w = 600 MPa, max. volume flow rate Q_w = 2.8 l/min). A total of three cutting heads were used. To represent normal job shop operation, a standard cutting head commonly used in industry was employed. This was equipped with a common nozzle combination (manufacturer BFT, type TJ006070/591, d_o = 0.28 mm, d_f = 0.76 mm, l_f = 70 mm), in the following referred to as "Macro". To represent common micro-cutting applications, the nozzle combination used was: d_o = 0.125 mm, d_f = 0.3 mm, l_f = 32 mm. The use of two different cutting heads was necessary in order to provide the best possible nozzle centering on the one hand, but also providing the necessary sealing for pressures $p \geq 450$ MPa on the other. The cutting heads used were a self-centering one for operating pressures of $p \leq 350$ MPa (IW Hannover / Dick & Dick GmbH, referred to as "Micro A") and a statically centering one for operating pressures $p \geq 450$ MPa (manufacturer Allfi, type Centerline II, referred to as "Micro B"). All water orifices were sapphires (manufacturer Comadur); all focusing tubes were made of tungsten carbide (manufacturer Ceratizit, type WJNS/Standard).

3.2 Cutting performance benchmark

Prior to the jetting experiments, the cutting performance of the Micro and Macro cutting systems was benchmarked by kerf tests with wedge-shaped specimen. The feed rate was oriented from the summit into the specimen. The tests were carried out with five different abrasive mass flow load ratios (5 %, 10 %, 15 %, 20 % and 25 % by weight), which allowed for the determination of cutting power at different loading situations. In most industrial applications, an abrasive/water load ratio between 0.18 and 0.20 by weight has been evaluated as very economical. Dependent on the particle size mixture, a certain saturation level can already exist on lower abrasive/water proportions. The applied investigation method not only provides for a benchmark of the abrasives but only allows for an estimation of the optimum abrasive/water load ratio.

The tests were carried out with stainless steel specimen (DE 1.4301, similar to AISI 304) and a wedge angle of $\alpha = 15°$. The feed rate was kept constant at $f = 100$ mm/min, and two pressure levels were employed ($p_2 = 350$ MPa and $p_4 = 550$ MPa).

3.3 Jetting experiments

This test series was carried out in order to investigate the abrasive particle disintegration in the jet forming process; all experiments were carried out without a work piece. For the experiments, abrasive collecting vessels according to Figure 2 were constructed. Prior to the experiments, the vessels were completely filled up with water. The focusing tube of the cutting head was positioned slightly underneath water level before the experiment was started for a determined test duration. The different abrasive load ratios and nozzle sizes required varying test durations; for a required balancing weight of $m_b = 30$ g, the test duration was always set individually to receive a minimum of $m_a = 150$ g of abrasive in the vessel. After each experiment, the vessel was removed and the abrasive was left for sedimentation for a couple of days. The sedimentation was controlled optically through laterally inserted inspection glasses. After sedimentation, the excessive water was carefully decanted and the garnet specimens were subject to a further drying process in a heat treatment furnace at a temperature of $T_f = 200$ °C (392 °F) for a minimum duration of $t_f = 8$ h. According to DIN 66165 (12), the balancing weight was chosen as $m_b = 30$ g for a sieve diameter of $d_s = 200$ mm and an abrasive bulk mass of $m'_b = 2{,}3$ g/cm³. The sieving duration was experimentally determined to be $t_s = 20$ min, which also corresponds to the guide value in Ref. (13).

The experiments were carried out with the “Macro” and “Micro” cutting heads for the pressure levels of $p_1 = 250$ MPa, $p_2 = 350$ MPa, $p_3 = 450$ MPa and $p_4 = 550$ MPa and five different abrasive mass flow load ratios (5 %, 10 %, 15 %, 20 % and 25 % by weight).

A sieve analysis initially results in a cumulative distribution of the mesh sizes. A linear diagram mostly leads to an S-shaped curve progression, which cannot easily be adapted for a statistical analysis. According to (13,14), three distribution functions may be used for the graphic presentation of particle size distributions. These include the power function (15), the log-normal distribution (16,17) and the Weibull distribution (RRSB function) (18). For a sieve analysis with a wide particle size distribution and a high fine particle share, the log-normal distribution is considered most suitable.

Initially, the quantities are plotted as cumulative distribution Q_r. For every sieve run R, equation (3.3.1) applies:

$$R = \frac{subset\ (which\ passes\ a\ sieve\ with\ given\ mesh\ size\ w)}{total\ quantity\ (of\ the\ sieve\ job)} \quad [-] \quad (3.3.1)$$

The sieve grades represent an interval of particle sizes Δx_i, therefore the arithmetic mean of its interval width $\bar{x}_i$ is characteristic for this particle class.

$$\Delta x_i = x_i - x_{i-1} \quad [\mu m] \quad (3.3.2)$$

$$\bar{x}_i = \frac{x_i + x_{i-1}}{2} \quad [\mu m] \quad (3.3.3)$$

For each run R and each mean particle size of the intervals $\bar{x}_i$, the distribution density $q_{r,i}$ represents the mass fraction that remains between two sieves.

$$q_{r,i} = \frac{subset\ \ x_{i-1} \dots x_i}{total\ quantity * interval\ width} \quad [\mu m^{-1}] \quad (3.3.4)$$

According to (14), the amount type r is set to r = 3 for mass and volume distributions. To analyze the size distribution of each sieve run R in a better way, the following mean values were used. The median value $x_{50,3}$ describes a particle size, which is bigger than 50% of the total particles. The mode $x_{h,3}$ is defined as the most common particle size. The mean particle size $\bar{x}_3$ indicates the weighted mean in relation to the occurring mass fraction.

$$\bar{x}_3 = \sum_{i=1}^{n} \bar{x}_i * R \quad [\mu m] \quad (3.3.5)$$

According to (13,14,16), the log-normal distribution is suitable for this application and was therefore used for the further analysis. In this distribution type, the logarithm of the particle size is normally distributed. As a 2-parameter approximation for the measured size distribution, the function gives a simple illustration of the distribution. The distribution density $q_3(x)$ results from equation (3.3.6):

$$q_3(\mathrm{x}) = \frac{1}{\sigma_{ln}\sqrt{2\pi}} \cdot \frac{1}{x} \cdot exp\left[-\frac{1}{2}\left(\frac{\ln(x/x_{50,3})}{\sigma_{ln}}\right)^2\right] \quad [\mu m^{-1}] \quad (3.3.6)$$

According to equation (3.3.7), the standard deviation can be calculated (16) as

$$\sigma_{ln} = \frac{1}{2} \cdot ln\frac{x_{84}}{x_{16}} \quad [-] \quad (3.3.7)$$

where the values for x_{16}, x_{84} and $x_{50,3}$ are obtained from the cumulative distribution graph.

By utilization of equations (3.3.8) and (3.3.9), the specific surface S_V and the Sauter mean diameter d_{32} can be calculated. Hereby, f indicates the so-called Heywood factor for different grain shapes. Based on past investigations of abrasives for industrial customers, a mean value of f = 1.8 was used in this calculation. The Sauter mean diameter indicates the equivalent diameter of a ball with a similar surface compared to the particle.

$$S_V = \frac{6f}{x_{50,3}} \cdot exp\frac{\sigma_{ln}^2}{2} \quad [\mu m^2] \quad (3.3.8)$$

$$d_{32} = \frac{6}{S_V} \quad [\mu m] \qquad (3.3.9)$$

The mode $x_{h,3}$ of the log-normal distribution is given by

$$x_{h,3} = x_{50,3} \cdot exp[-\sigma_{ln}^2] \quad [\mu m] \qquad (3.3.10)$$

Fine particles can supersaturate the AWIJ without providing an increased cutting power. The fine particle fraction is determined with regard to analytical methods for soil samples derived from geoscience (19). The fine particle share ≤ 63 µm is considered separately in the results.

3.4 Cutting experiments

The procedure of the cutting experiments was similar to that of the previously described jetting experiments (3.3). The main difference comprises that the jet was not immediately dissipated after formation but was used for a defined cutting process. As test material, unalloyed construction steel (DE 1.0503, similar to AISI 1045) with a thickness of t_1 = 10 mm for macro applications and t_2 = 3 mm for micro applications was used. An unalloyed engineering steal was intentionally chosen in order to remove the metal chipping from the used abrasive magnetically. To ensure a similar grade of abrasive stress between the different loading situations, orifice sizes and pressure levels, the feed rates were calculated individually regarding to (5) for a cutting quality of q = 3. The calculation based on (5) was preferred as compared to (6), because the consideration of pressure-dependent water density is not possible with the latter. The specimens were mounted in the abrasive vessels according to Figure 2 (D) and covered with a water level of t_w = 10 mm prior to the experiment in order to avoid reflections. Data acquisition and analysis were carried out identically to the previously described jetting experiments (3.3).

4. RESULTS

4.1 Raw material sieve analysis

The sieve analysis results of the unused garnets are displayed in Figure 3. Both abrasives meet their manufacturer's specifications, the distribution curves are almost identical to ones given in the data sheets. The most common particle size for GMA #120 is 180 µm; the most common size for Barton #220 is 90 µm.

4.2 Cutting performance benchmark

The results of the carried-out kerf tests are displayed in Figure 4. According to (20), the cutting performance P_s is calculated from kerf depth k_s and feed rate f:

$$P_s = k_s \cdot f \quad [mm/s] \qquad (4.2.1)$$

For the Macro system, optimum load ratios of $R_{macro,350}$ = 0.19 (p_2 = 350 MPa) and $R_{macro,350}$ = 0.21 (p_4 = 550 MPa) were determined. The load ratio values for the Micro system are slightly lower and amount to $R_{micro,350}$ = 0.17 (p_2 = 350 MPa) and $R_{micro,350}$ = 0.19 (p_4 = 550 MPa). The cutting performance of the micro system at high pressure approximately corresponds to the macro system at lower pressure. Hydraulic power P_w is however significantly different in both cases

($P_{w,micro,550}$ = 4,38 kW and $P_{w,macro,350}$ = 11,42 kW), therefore the effectivity of particle acceleration seems to be higher for the micro jet.

4.3 Jetting Experiments

A plot of log-normal distribution curves is displayed in Figure 5 for the case of macro cutting. In the table attached, the associated data (median value $x_{50,3}$, standard deviation σ_{ln}, mode $x_{h,3}$, mean particle size $\bar{x}_3$ and Sauter mean diameter $d_{3,2}$) are displayed. A decrease of the particle size for higher pressure levels can be discerned from in both cases (macro and micro cutting). Simultaneously, the fine particle share increases. The same behavior can be recognized for the 8 other test, with only slight differences between the experimental series. The maximum mean particle size occurs at the lowest pressure levels (p_1 = 250 MPa) while the highest pressure (p_4 = 550 MPa) effects the minimum mean particle sizes. For the micro cutting experiments, the standard deviation is slightly higher for cutting system "Micro B" (p_3 = 450 MPa, p_4 = 550 MPa), this can be seen by the flatter curve progession. This can be attributed to the better orifice - focusing tube alignment of the cutting system "Micro A".

4.4 Cutting Experiments

As stated in section 3.4, the test material (DE 1.0503, similar to AISI 1045) was intentionally chosen in order to remove the metal chipping from the used abrasive magnetically. However, different attempts to separate the micro chipping from the abrasive failed, even the installation of magnets in the sieve shaker did not separate the chipping from the abrasive grains. In Figure 6 A, several pictures of used abrasive with metal chipping with an approaching magnet are displayed. A higher magnification image is shown in Figure 6 B. The metal chipping aligns along the magnetic field and entrains the abrasive grains. The further analysis therefore had to be carried out with the attached particles. For abrasive grains with agglomerating chipping, the apparent grain size increases. In Figure 7, SEM- and photomicroscopic micrographs of single particles after the cutting experiment are displayed. The potential error regarding the chipping is considered to be low, because the microscopic pictures indicate considerably smaller chip sizes compared to the grain sizes. This error therefore mainly affects the fine fraction.

A representative plot of log-normal distribution curves is displayed in Figure 8 for micro cutting. In the attached table, the associated data (median value $x_{50,3}$, standard deviation σ_{ln}, mode $x_{h,3}$, mean particle size $\bar{x}_3$ and Sauter mean diameter $d_{3,2}$) are summarized. Overall, the results correspond to those from the jetting experiments. The maximum mean particle size occurs at the lowest pressure levels (p_1 = 250 MPa), while higher pressure effects the minimum mean particle sizes. However, compared to the jetting experiments, some deviations between the experimental series become obvious, which possibly can be attributed to the mentioned effect through chipping adhesion. The mean values, however, do not indicate an additional significant particle disintegration through the cutting process.

5. DISCUSSION

A possible explanation for the effect of metal chipping agglomeration on the abrasive grains is an increasing electrostatic chargeability for small particle sizes. According to (13), smaller grain sizes

tend to agglomeration and wall adhesion. Compared to the jetting experiments, some deviations between the log-normal distribution curves of some experimental series became apparent. This can probably be attributed to the mentioned effect through chipping adhesion.

The plots of the mean particle size $\bar{x}_3$ of the particles > 63 µm from the jetting experiments are displayed in Figure 9 (macro cutting) and Figure 10 (micro cutting). In the case of micro cutting, the graph is split in the middle in order to make clear that two cutting heads with different centering mechanisms have been used. Considering the experimental data displayed in the figures, the influence of pressure clearly becomes apparent for both micro and macro systems. Higher pressure directly reduces the particle size. This tendency has been previously reported (2). The load ratio has less influence on particle disintegration. While for the macro system, a decrease of particle size for an increasing load ratio is still clearly recognizable, this effect is not big enough to become apparent in the experimental data of the micro system. A further, significant particle disintegration through the cutting process could not be detected, this corresponds to the results of the related investigation in Ref. (2).

The fine particle fraction (share of particles ≤ 63 µm) is plotted in Figure 11 (macro cutting) and Figure 12 (micro cutting). A distinct tendency to an increasing fine particle share for increasing pressure can be recognized. The influence of an increasing abrasive load ratio is only minor, but it can also be found to increase the fine particle share.

The decrease of the mean particle size $\bar{x}_3$ is calculated from the mean particle size $\bar{x}_{3,s}$ of the experimental series s and the mean particle size $\bar{x}_{3,n}$ of the new condition grains. This can also be referred to as "degree of particle disintegration", D.

$$D = \frac{\bar{x}_{3,s}}{\bar{x}_{3,n}} \quad [\%] \qquad (5.1)$$

In Figure 13, the degree of particle disintegration D is plotted for several pressures. The influence of pressure clearly becomes apparent here for both systems. An important finding is that D is consistently lower for micro cutting systems. Noticeable are the similar experimental values for $D_{micro,550}$ and $D_{macro,350}$. Considering Figure 4, the curve progression of the cutting performance is also almost identical. It seems likely that D is generally dependent on the particle momentum, equally if the particle velocity is provided by big orifices or high pressure. A higher degree of particle disintegration does not only have an effect on cutting performance, but also on lifetime of the focusing tube. The most significant amount of particle disintegration takes place in the jet forming process. Disintegration can take place either in mixing chamber and the focusing tube inlet guiding cone or the focusing tube cylinder. The ratio of disintegration in these places is, however, hard to determine. Disintegration in the mixing tube and inlet cone can possibly be reduced by delivery of the abrasive in jet direction or an in-process deflection of the abrasive delivery, maybe also through optimized inlet cones.

6. ACKNOWLEDGEMENTS

The authors thank the German Working Group of Waterjet Technology (AWT) for fruitful discussion.

7. REFERENCES

1. Henning, A. Modelling of the kerf geometry with abrasive waterjet cutting: Modellierung der Schnittgeometrie beim Schneiden mit dem Wasserabrasivstrahl; Jost-Jetter: Heimsheim, 2008.
2. Ohlsen, J. Recycling von Feststoffen beim Wasserabrasivstrahlverfahren; VDI-Verl.: Düsseldorf, 1997.
3. Hashish, M. A Modeling Study of Metal Cutting With Abrasive Waterjets. J. Eng. Mater. Technol. 1984, 106, 88.
4. Hashish, M. A Model for Abrasive-Waterjet (AWJ) Machining. J. Eng. Mater. Technol. 1989, 111, 154.
5. Zeng, J.; Kim, T. Parameter Prediction and Cost Analysis in Abrasive Waterjet Cutting Operations; Proceedings of the 7th American WJTA Conference, August 19-21, Seattle, Washington., 1993.
6. Zeng, J. Determination of machinability and abrasive cutting properties in AWJ cutting; Proceedings of the 2007 American WJTA Conference and Expo, August 19-21, Houston, Texas., 2007.
7. Lichtarowicz, A., Ed. Jet Cutting Technology; Springer Netherlands: Dordrecht, 1992.
8. Hoogstrate, A.M.; Karpuschewski, B.; van Luttervelt, C.A.; Kals, H. Modelling of high velocity, loose abrasive machining processes. CIRP Annals - Manufacturing Technology 2002, 51, 263–266.
9. GMA Garnet Group. GMA GARNET. Das natürliche Wasserstrahlschneidemittel. Produktdatenblatt, 2009.
10. Barton International. HPX® Fine Waterjet Abrasives Typical Particle Size Distribution. Graph and Table: Glen Falls, NY, USA, 2011.
11. DIN ISO 565. DIN Deutsches Institut für Normung e.V. Test sieves - Metal wire cloth, perforated metal plate and electroformed sheet - Nominal sizes of openings, 1998.
12. DIN 66165. DIN Deutsches Institut für Normung e.V. Partikelgrößenanalyse, Siebanalyse. Teil 1: Grundlagen; Teil 2: Durchführung, 1987.
13. Stiess, M. Mechanische Verfahrenstechnik: Partikeltechnologie, 3rd ed; Springer Berlin Heidelberg: Berlin, Heidelberg, 2009.
14. DIN ISO 9276. DIN Deutsches Institut für Normung e.V. Representation of results of particle size analysis - Part 1: Graphical representation; Part 2: Calculation of average particle sizes/diameters and moments from particle size distributions; Part 4: Characterization of a classification process; Representation of results of particle size analysis, 2004-2012.
15. DIN 66143. DIN Deutsches Institut für Normung e.V. Darstellung von Korn-(Teilchen-) größenverteilungen. Potenznetz, 1974.
16. DIN 66144. DIN Deutsches Institut für Normung e.V. Darstellung von Korn-(Teilchen-) größenverteilungen. Logarithmisches Normalverteilungsnetz, 1974.
17. ISO 9276-5. ISO - International Organization for Standardization. Representation of results of particle size analysis - Part 5: Methods of calculation relating to particle size analyses using logarithmic normal probability distribution, 2005.
18. DIN 66145. DIN Deutsches Institut für Normung e.V. Darstellung von Korn-(Teilchen-) größenverteilungen. RRSB-Netz, 1976.

19. DIN 18123. DIN Deutsches Institut für Normung e.V. Soil, investigation and testing - Determination of grain-size distribution, 2011.
20. Peter, D. Untersuchungen zu Einsatzmöglichkeiten von Wasserabrasivstrahlen für Rückbaumaßnahmen; PZH, Produktionstechn. Zentrum: Garbsen, 2007.
21. Barton International. Technical Data & Physical Characteristics for Hard Rock Garnet Abrasives: Glen Falls, NY, USA, 2012.

8. TABLES

Table 1: Garnet product data (9,21)

Product labeling	GMA Garnet #120	Barton Garnet HPX #220
Relative density	4.1	3.9
Mohs hardness	7.5 – 8.0 Mohs	7.5 – 8.5 Mohs
Melting point	1250 °C (2282 °F)	1315 °C (2399 °F)
Electric conductivity (max.)	25 ms/m	25 ms/m
Almadine content	97 % - 98 %	92 % - 96 %

9. FIGURES

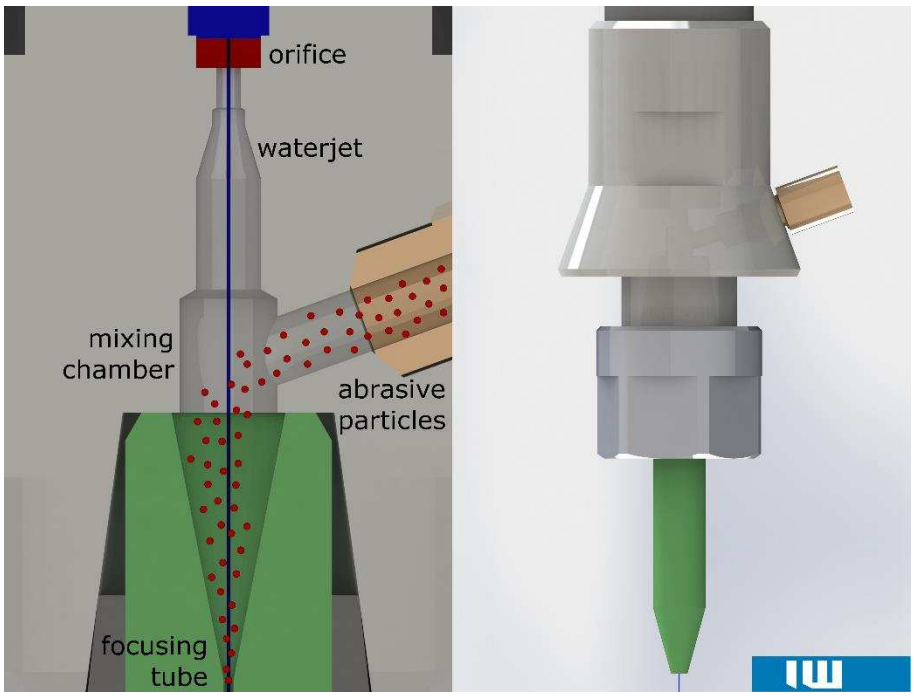

Figure 1: Schematic AWIJ cutting head

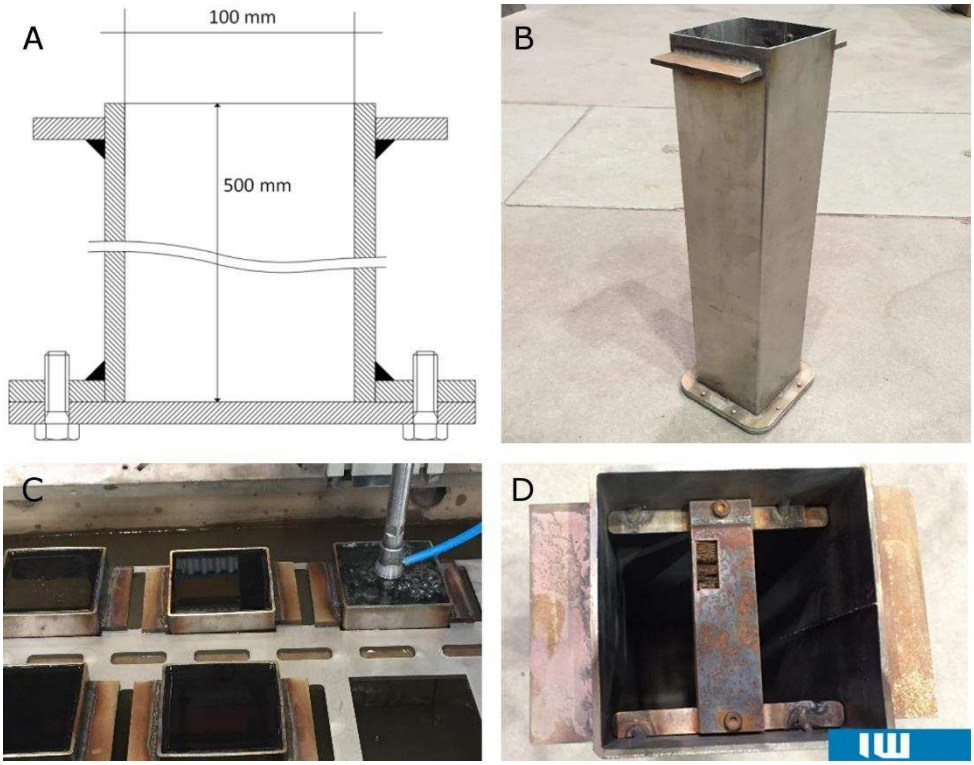

Figure 2: Abrasive collecting vessel (A-B), Jetting experiment with mounted vessels (C), mounted specimen for cutting experiments (D)

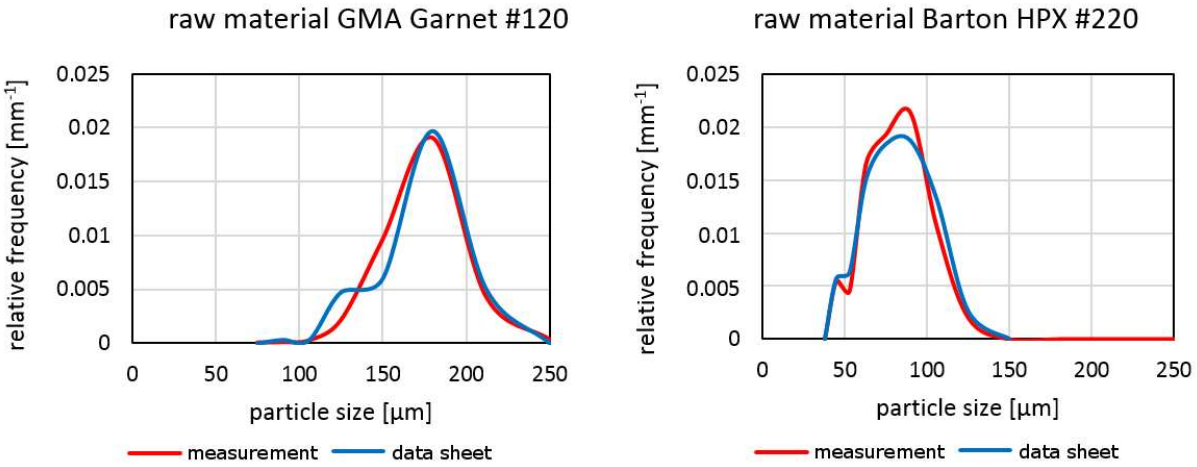

Figure 3: Abrasive sieve analysis according to ISO 565, R40/3 (11) prior to the jet formation (red), and particle size distribution as given by the manufacturers (blue) (9,10)

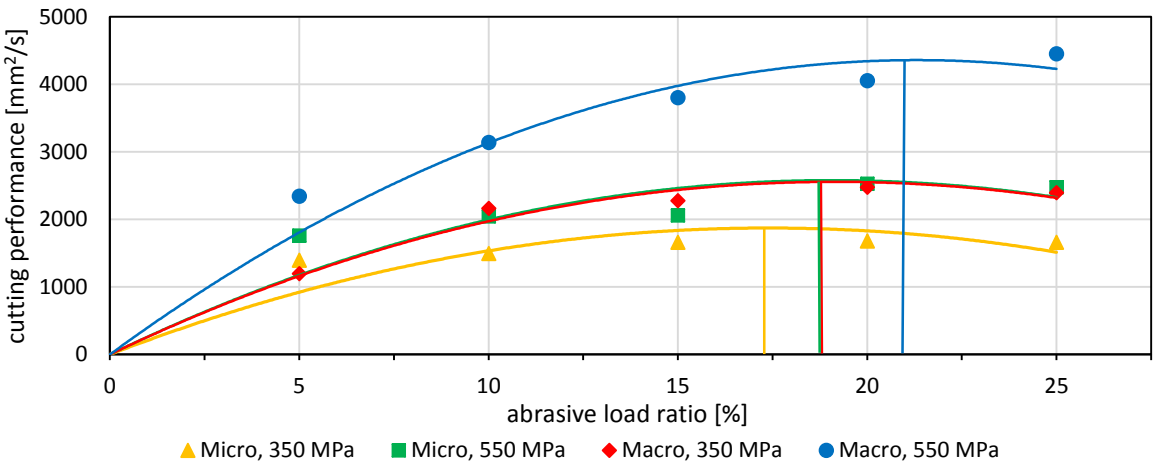

Figure 4: Cutting performance for different abrasive load ratios and operating pressures

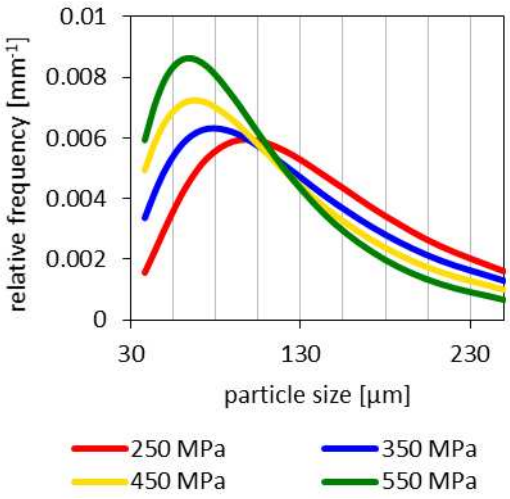

p [MPa]	250	350	450	550
$x_{50,3}$ [µm]	137	120	104	92
σ_{ln}	0,58	0,65	0,66	0,60
$x_{h,3}$ [µm]	98	79	68	64
$\bar{x}_3$ [µm]	129	115	107	100
$d_{3,2}$ [µm]	64	54	47	43
Fine fraction: < 63 µm [%]	14	20	23	23
$\bar{x}_3$ > 63 µm [µm]	144	135	130	120

Figure 5: Exemplary log-normal distribution curves for a jetting experiment with the macro system. d_o = 0,28 mm, d_f = 0,76 mm, R = 15 %

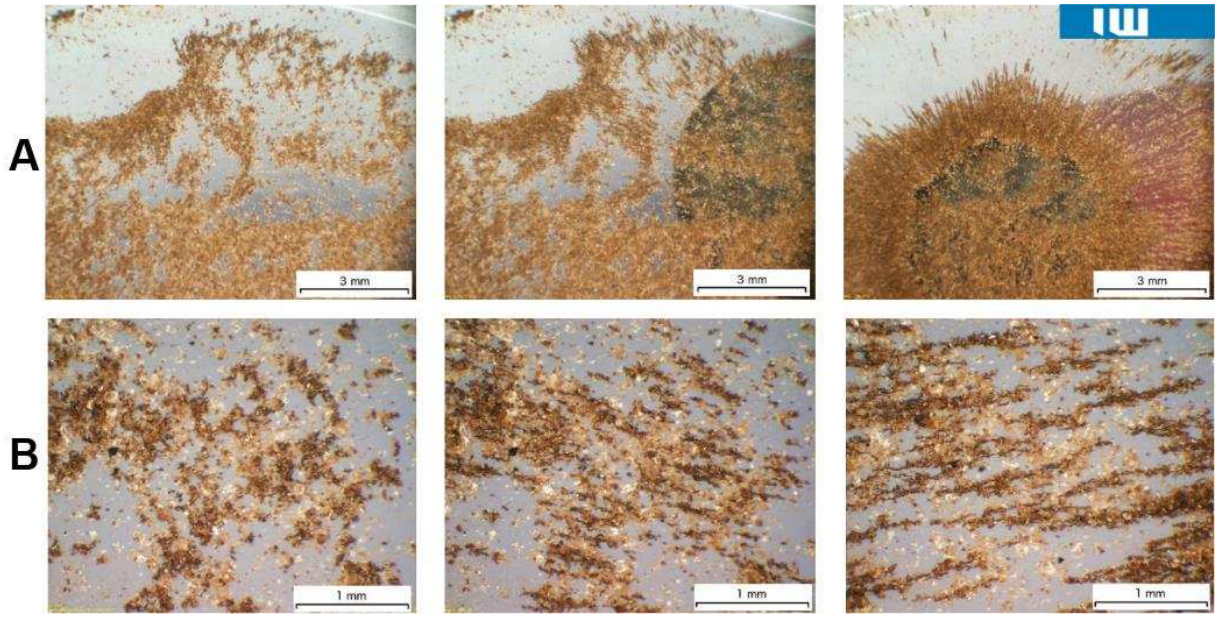

Figure 6: Photomicrographs of abrasive with attached, magnetic micro chipping

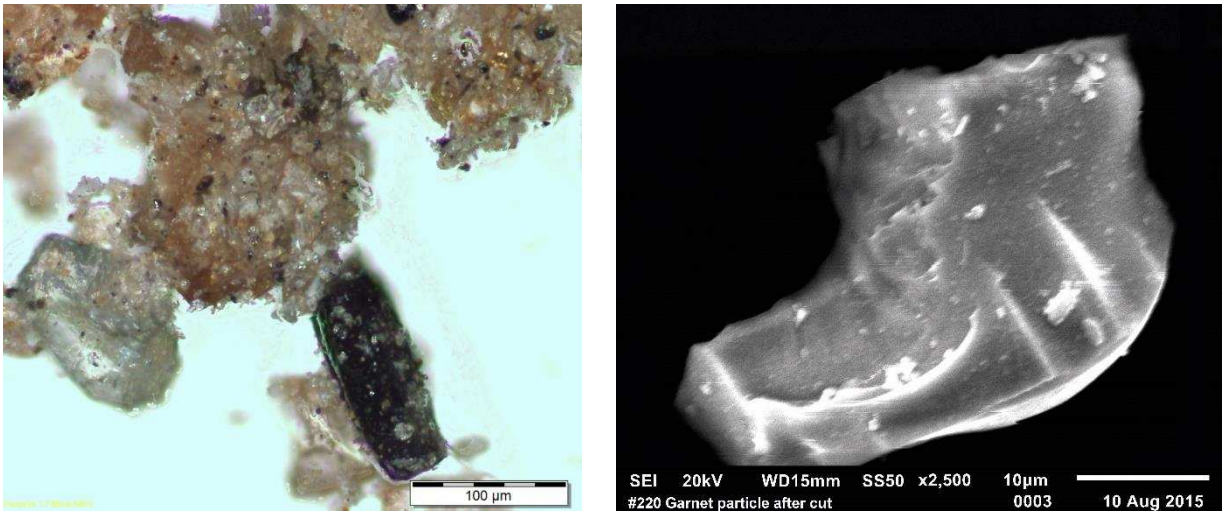

Figure 7: Photomicrograph and SEM-micrograph of disrupted abrasive particles (Barton HPX #220 after cutting experiment)

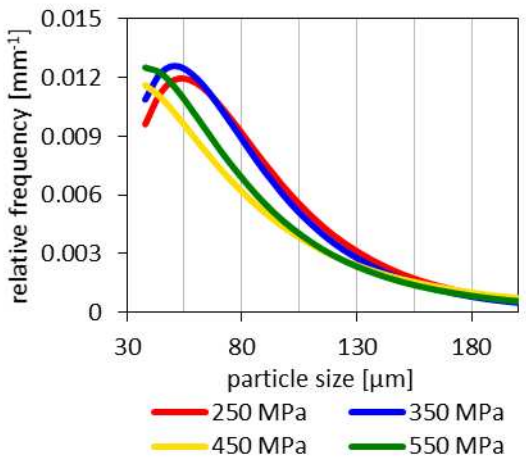

p [MPa]	250	350	450	550
$x_{50,3}$ [µm]	72	68	60	60
σ_{ln}	0,53	0,54	0,75	0,66
$x_{h,3}$ [µm]	54	51	34	39
$\bar{x}_3$ [µm]	69	64	58	58
$d_{3,2}$ [µm]	35	33	25	27
Fine fraction: < 63 µm [%]	29	37	45	46
$\bar{x}_3$ > 63 µm [µm]	85	84	82	82

Figure 8: Exemplary log-normal distribution curves for a cutting experiment with the micro system. d_o = 0,125 mm, d_f = 0,3 mm, R = 20 %

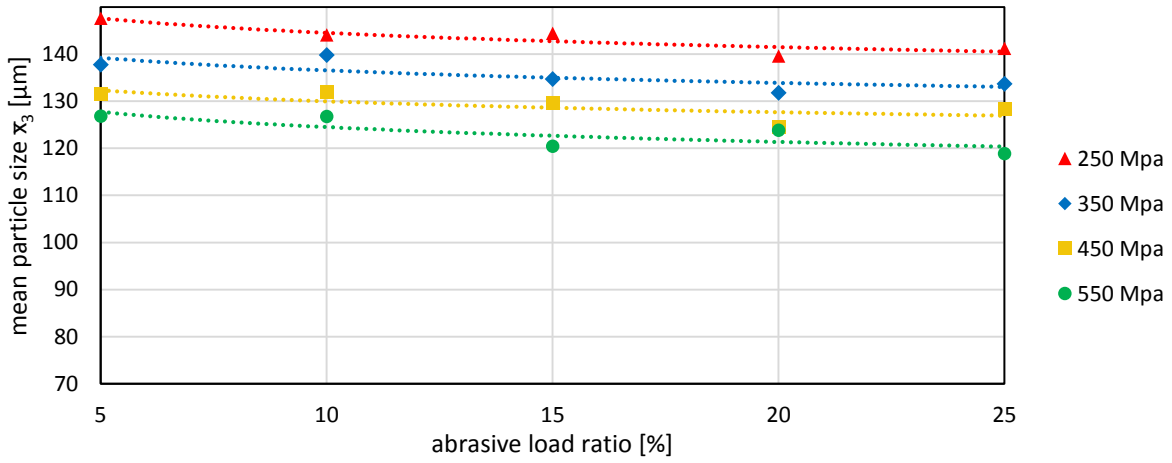

Figure 9: Plot of the mean particle size (> 63 µm) after jet formation (macro cutting)

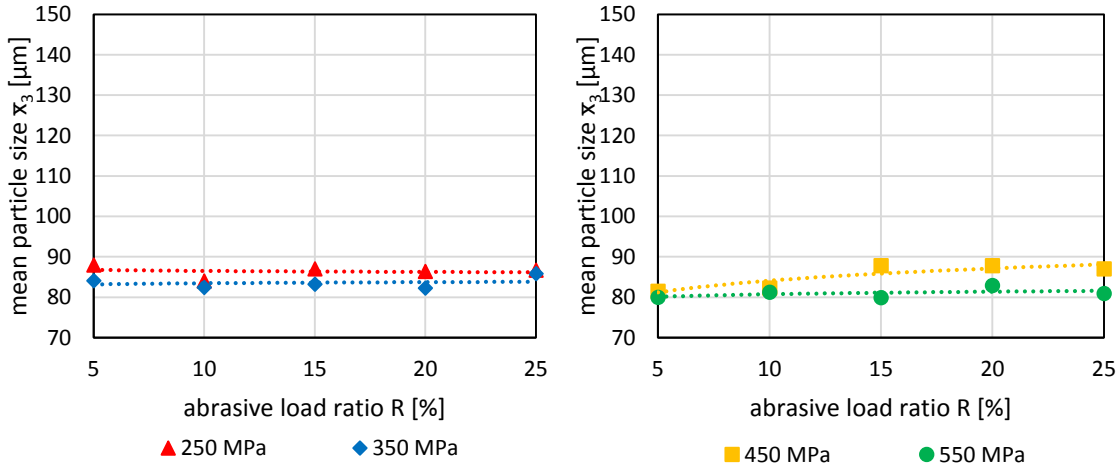

Figure 10: Plots of the mean particle size (> 63 µm) after jet formation (micro cutting)

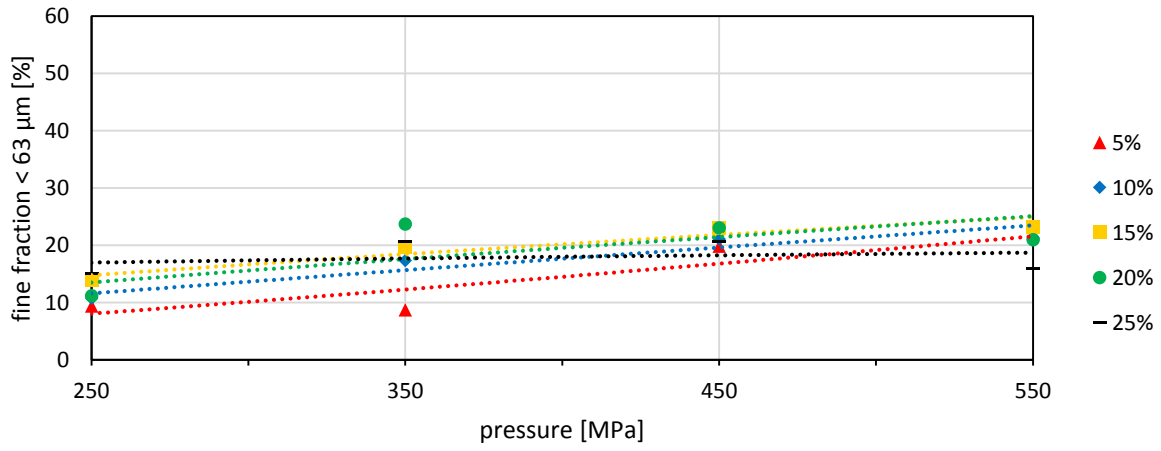

Figure 11: Plot of the fine particle fraction, macro cutting

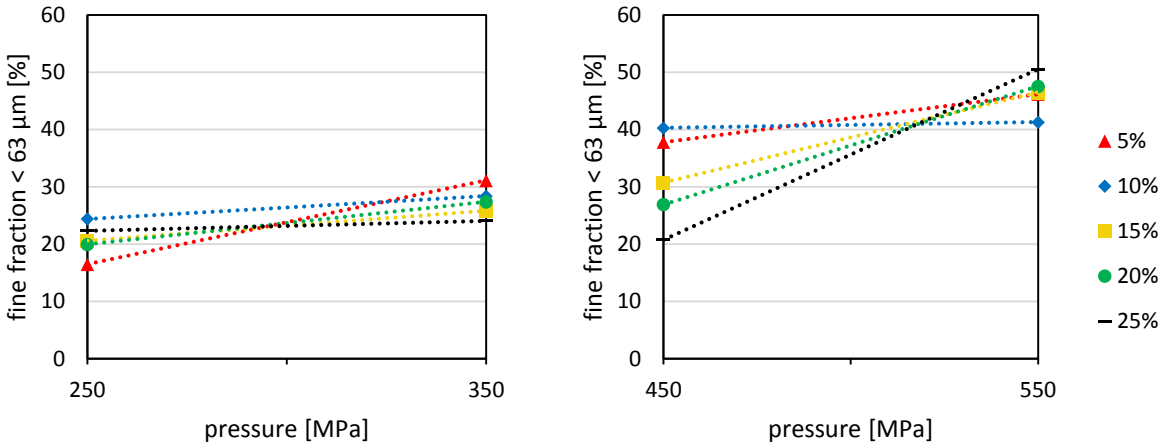

Figure 12: Plots of the fine particle fraction, micro cutting

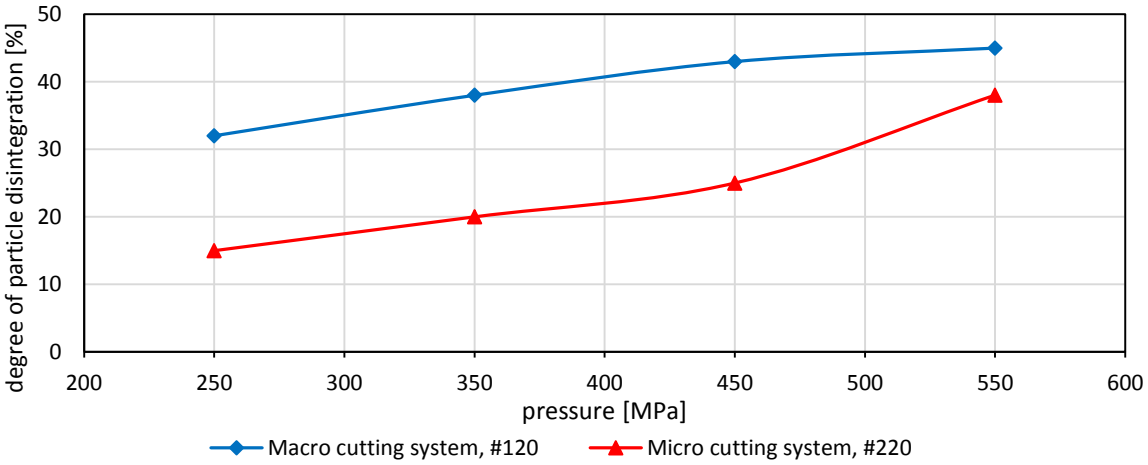

Figure 13: Degree of particle disintegration D for different pressures